Proton Release Due to Manganese Binding and Oxidation in Modified Bacterial Reaction Centers†

L. Kálmán,‡ M. C. Thielges,‖,§ J. C. Williams,‖ and J. P. Allen*,‖

Department of Chemistry and Biochemistry, Arizona State University, Tempe, Arizona 85287-1604, and Department of Physics, Concordia University, Montreal, Quebec H4B 1R6, Canada

Received June 14, 2005; Revised Manuscript Received August 2, 2005

ABSTRACT: The pH dependence of binding and oxidation of Mn^{2+} in highly oxidizing reaction centers with designed metal-binding sites was characterized by light-minus-dark optical difference spectroscopy and direct measurements of proton uptake/release. These mutants bind a Mn^{2+} ion that can efficiently transfer an electron to the oxidized bacteriochlorophyll dimer, as described earlier [Thielges et al. (2005) *Biochemistry 44*, 7389−7394]. The dissociation constant, K_D, significantly increased with decreasing pH. The pH dependence of K_D between pH 7 and pH 8 was consistent with the binding of Mn^{2+} being stabilized by the electrostatic release of two protons. The strong pH dependence of proton release upon Mn^{2+} binding, with a maximal release of 1.4 H^+ per reaction center, was interpreted as being a result of a shift in the pK_a values of the coordinating residues and possibly other nearby residues. A small amount of proton release associated with Mn^{2+} oxidation was observed upon illumination. These results show that functional metal-binding sites can be incorporated into proteins upon consideration of both the metal coordination and protonation states of the ligands.

Manganese is an essential trace element and can have many different functions in proteins. Because manganese is redox-active under physiological conditions, it often plays an important role in biological redox reactions, for example, in enzymes such as manganese superoxide dismutase, manganese peroxidase, manganese-containing ribonucleotide reductase, and manganese catalase. In these enzymes the redox activity of the manganese center is established primarily through the coordination of the manganese to the protonatable amino acid residues histidine, aspartate, and glutamate, with water also usually present (*1*−*3*).

Manganese plays a critical functional role in photosystem II but not in the evolutionarily related bacterial reaction center (*4*, *5*). In both complexes, light initiates a transmembrane charge separation from the electron donor, the bacteriochlorophyll dimer, P,[1] in bacterial reaction centers or the chlorophyll cofactor P680 in photosystem II, to the quinones, Q_A and Q_B, acting as electron acceptors, in a process that is coupled to the transfer of protons (*6*, *7*). However, three key characteristics of photosystem II provide this complex with the unique ability to oxidize water to molecular oxygen. First, P680 is highly oxidizing with an oxidation/reduction midpoint potential over 1 V. Second, the electron transfer process from the manganese cluster to P680 is coupled to proton transfer through the involvement of a redox-active tyrosine. Finally, photosystem II contains a manganese cluster that can collect the four electron equivalents needed for water oxidation.

Modifications of reaction centers from *Rhodobacter sphaeroides* have been performed in order to incorporate these key functional features. By systematically changing the hydrogen-bonding pattern of P, the P/P^+ potential was elevated substantially to create highly oxidizing reaction centers (*8*). Tyrosine residues were incorporated in the highly oxidizing reaction centers at positions corresponding to the redox-active tyrosines of photosystem II and found to be capable of coupling electron and proton transfer (*9*−*13*). These highly oxidizing reaction centers were able to oxidize manganese(II) but only as a second-order diffusion-controlled process (*14*). Four different manganese-binding sites were designed at a location analogous to that of photosystem II in reaction centers that also contained the alterations producing a highly oxidizing electron donor (*15*). The three-dimensional structure solved for one of these mutants showed that the manganese was bound at the designed site (Figure 1). Different dissociation constants were found for manganese binding in the mutants using steady-state absorption measurements. The bound manganese was capable of efficiently reducing P^+ in a first-order process, and the relative amplitude of this component yielded dissociation constants that agreed with those determined using the steady-state experiments. In this study, the pH dependence of manganese binding and oxidation in these mutants was correlated with the pH dependence of the amount of protons released upon manganese binding. Also, the proton uptake/release upon oxidation of the bound manganese was measured and related to the protonation states of the residues at the manganese-binding site.

† This work was supported by Grant MCB 0131764 from the NSF.

* Corresponding author. Phone: 480-965-8241. Fax: 480-965-2747. E-mail: jallen@asu.edu.

‡ Concordia University.

§ Present address: The Scripps Research Institute, La Jolla, CA.

‖ Arizona State University.

[1] Abbreviations: P, bacteriochlorophyll dimer; P680, chlorophyll donor of photosystem II; Q_A and Q_B, primary and secondary quinones, respectively.

10.1021/bi051149w CCC: $30.25
Published on Web 09/16/2005

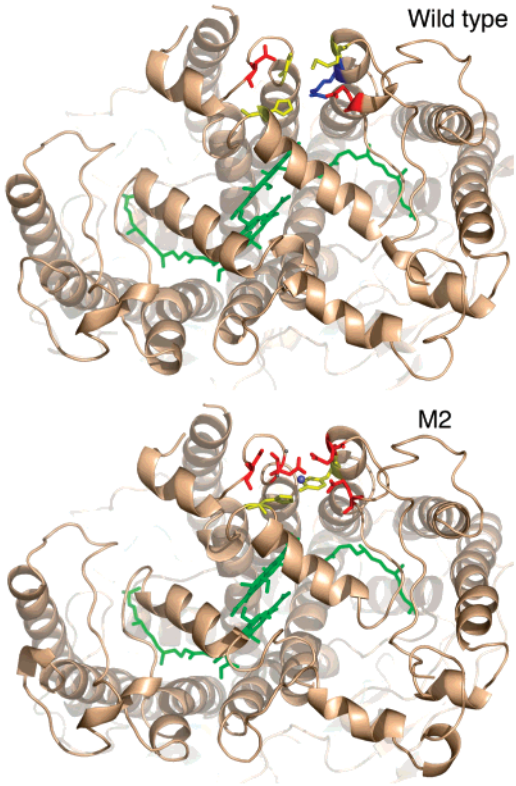

FIGURE 1: Structural representation of the reaction center from the wild type (upper) and the M2 mutant (lower) as viewed from the periplasmic side. The M2 mutant shows the Mn^{2+}-binding pocket with the Mn^{2+} ion (purple sphere), the nearby residues Tyr M164 (yellow), Glu M168 (red), Glu M173 (red), His M193 (yellow), Asp M288 (red), and Glu M292 (red), and two bound water molecules (gray spheres). The corresponding region in the wild type contains residues Arg M164 (blue), Met M168 (yellow), Glu M173 (red), His M193 (yellow), Gly M288 (yellow), and Glu M292 (red). Also shown in both structures are the backbone (brown) and P (green). For the residues shown, negatively charged residues (Glu and Asp) are indicated with red, the positively charged residue (Arg) is in blue, and neutral residues are in yellow. Coordinates for the wild type are from PDB file 1M3X, and coordinates for the M2 mutant are from PDB file 1Z9J. The structural representation was made using PYMOL (*16*).

MATERIALS AND METHODS

Construction of Mutants, Protein Isolation, and Sample Preparation. The construction of the control and the M1−M4 mutants has been described previously (*15*). Each of these mutants contains three amino acid substitutions that produce a highly oxidizing reaction center, Leu L131 to His, Leu M160 to His, and Phe M197 to His, as well as the mutation Arg M164 to Tyr that introduces a Tyr near the manganese-binding site. In addition to these four changes, the M1−M4 mutants contain the following substitutions: Met M168 to Glu and Val M192 to Glu in the M1 mutant, Met M168 to Glu and Gly M288 to Asp in the M2 mutant, Val M192 to Glu and Gly M288 to Asp in the M3 mutant, and Met M168 to Glu, Val M192 to Glu, and Gly M288 to Asp in the M4 mutant. The M2-RY(M164) mutant is identical to the M2 mutant except that it does not contain the Arg M164 to Tyr substitution. It was constructed by site-directed mutagenesis and manipulation of restriction fragments as previously described (*8*), with the altered genes expressed in *R. sphaeroides* deletion strain ΔLM1.1 (*17*).

Cells were grown semiaerobically, and the reaction centers were prepared as described earlier, except that the nonionic detergent Triton X-100 was used for the ion exchange chromatography step instead of lauryl dimethylamine oxide (*18*). Any EDTA remaining in the preparation was removed by extensive dialysis. The assay solution for the pH dependence measurements contained 0.03% Triton X-100, 0 or 30 mM NaCl, and 15 mM 2-(*N*-morpholino)ethanesulfonic acid, *N*-(2-hydroxyethyl)piperazine-*N*′-2-ethanesulfonic acid, tris(hydroxymethyl)aminomethane, or 2-(*N*-cyclohexylamino)ethanesulfonic acid depending on pH. Measurements were performed in the presence of 100 μM terbutryne to block electron transfer from Q_A^- to Q_B unless otherwise stated.

Measurement of Absorption Changes. A Cary 5 spectrophotometer (Varian) was used to measure the optical absorbance changes induced by continuous illumination. The light excitation was achieved using an Oriel tungsten lamp with an 860 nm interference filter. The illumination lasted no longer than 30 s at any given time, and the intensity was set to approximately one-third of the saturating value of the wild type. The spectra were recorded using a fast scanning rate of 900 nm/min.

Proton Uptake/Release Measurements. The buffer [15 mM tris(hydroxymethyl)aminomethane hydrochloride] was removed by a long (24−48 h) dialysis against 0.05% Triton X-100 and 30 mM NaCl, pH 8.0. The pH of the buffer-free solution was set by adding aliquots of diluted HCl and NaOH solutions. The light-induced pH changes were measured using two independent methods. First, the pH changes were determined by measuring with a Cary 5 spectrophotometer the absorption changes of pH-sensitive dyes (bromocresol purple, pH 5.6−7.0; *o*-cresol red, pH 7.0−8.5; and *o*-cresol phthalein, pH 8.6−9.6) at approximately 586 nm, where the $PQ_A \rightarrow P^+Q_A^-$ transition has an isosbestic point. A magnetic stirrer was mounted under a custom cell holder in order to get a rapid distribution of added buffer or acid. Second, the pH changes were directly measured with a semimicro combination glass pH electrode (Corning Ross, 8103) connected to a pH meter (Orion SA 720). A differential amplifier of local design was used to amplify and electronically filter the signals. For direct measurements of the light-induced pH changes, excitation of the samples was achieved as described earlier (*19*).

The proton release associated with the binding of the manganese ions in the dark was measured with a pH electrode according to the method introduced by Gerencsér and Maróti (*20*). The net H^+ binding/release was determined at each pH value as the difference of the dye/electrode responses between the buffer-free and buffered (15 mM) samples. The following buffers were used: 2-(*N*-morpholino)ethanesulfonic acid, for pH 5.6−6.7; *N*-(2-hydroxyethyl)piperazine-*N*′-2-ethanesulfonic acid, for pH 7.0−8.0; tris(hydroxymethyl)aminomethane, for pH 7.6−8.8; and 2-(*N*-cyclohexylamino)ethanesulfonic acid, for pH 8.6−9.6. To determine the buffering capacity of the entire system, a known amount of strong acid (HCl) was added during extensive stirring of the sample solution. Absorption of carbon dioxide was prevented by the use of degassed solutions and saturating the gas phase over the samples with nitrogen gas. The samples contained 100 μM terbutryne to block electron transfer to Q_B. The total and photoactive

concentrations of the reaction centers were determined by monitoring the absorbance at 802 nm and the light-induced absorption changes at 865 and 450 nm, using the following extinction coefficients: $\epsilon_{802} = 288\ mM^{-1}\ cm^{-1}$, $\Delta\epsilon_{865} = 112\ mM^{-1}\ cm^{-1}$, and $\Delta\epsilon_{450} = 4.9\ mM^{-1}\ cm^{-1}$ (*21*−*23*). The ionic strength of the assay solution was optimized at 30 mM in order to obtain stable readings of the pH with a glass electrode and also to suppress possible electrochromic effects of the charge-separated states on some dye molecules. This level of ionic strength did not impair significantly the binding of manganese to the reaction centers.

Models and Fitting of the Observed pH Dependences. The fraction of P^+ at different pH values was measured by the extent of the light-induced absorption change at 865 nm. The value of the dissociation constant K_D was determined using the following equation introduced previously (*20*) and modified for use with these mutants (*15*):

$$\Delta A/\Delta A_0 = 1 - \{[Mn] + [RC] + K_D - \sqrt{([Mn] + [RC] + K_D)^2 - 4[RC][Mn]}\}/2[RC] + \Delta A_\infty/\Delta A_0 \quad (1)$$

where ΔA, ΔA_0, and ΔA_∞ are the absorption changes at 865 nm in the presence, in the absence, and in the highest concentration of Mn^{2+} ions, respectively, and [Mn] and [RC] are the total concentrations of Mn^{2+} and reaction centers, respectively. The ratio $\Delta A_\infty/\Delta A_0$ is included because the reduction of P^+ by bound Mn^{2+} may not be complete at all pH values.

The pH dependence of the values of K_D obtained using eq 1 was fitted using a previously introduced model that assumes metal binding to the ionized form of two protonatable amino acid residues (*20*, *24*):

$$K_D = (1 + 10^{pK_{a1}-pH} + 10^{pK_{a1}-pH}10^{pK_{a2}-pH})K_D^0 \quad (2)$$

where pK_{a1} and pK_{a2} are the negative logarithm values of the proton dissociation constants for the two protonatable amino acid residues and K_D^0 is the dissociation constant at high pH values where both residues are deprotonated. If the pK_{a1} and pK_{a2} values are equivalent within the error of the fit (±0.5 pH unit), then the model can be simplified using a single pK_{ac} value that is characteristic of the entire cluster:

$$K_D = (1 + 10^{pK_{ac}-pH} + (10^{pK_{ac}-pH})^2)K_D^0 \quad (3)$$

The pH dependence of proton release due to manganese binding can be fitted assuming a downshift, δpK_{ac}, in the pK_{ac} values of N residues of a cluster as a result of the electrostatic interaction with the divalent Mn^{2+} cation. The number of protons per reaction center, H^+/RC, released from N residues is given by

$$\frac{H^+}{RC} = \frac{N}{1 + 10^{pH-(pK_{ac}+\delta pK_{ac})}} - \frac{N}{1 + 10^{pH-pK_{ac}}} \quad (4)$$

RESULTS

Light-Induced Manganese Oxidation. In the absence of Mn^{2+}, light excitation results in the state $P^+Q_A^-$ in reaction centers as measured by the light-minus-dark optical spectrum in the 700−1000 nm region (Figure 2A). In the presence of

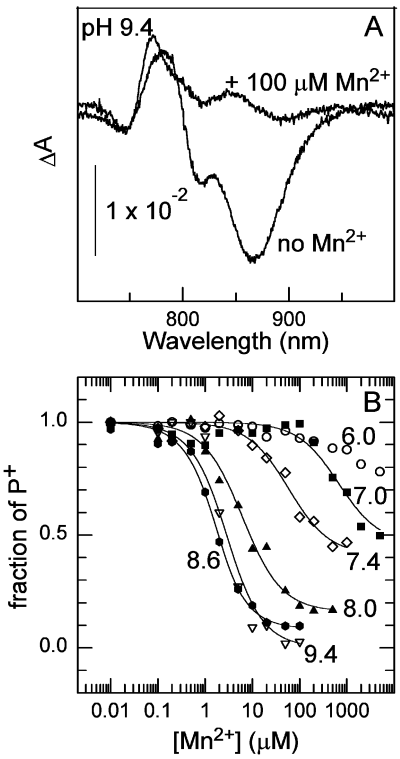

FIGURE 2: (A) Light-minus-dark difference optical spectra of the M2 mutant at pH 9.4 in the presence and in the absence of manganese. (B) Fraction of P^+ as a function of the added Mn^{2+} concentration at representative pH values measured in reaction centers from the M2 mutant at pH 6.0 (circles), pH 7.0 (squares), pH 7.4 (diamonds), pH 8.0 (triangles up), pH 8.6 (hexagons), and pH 9.4 (triangles down). The solid lines are the best fits to the experimental data points using eq 1. Below pH 7.0, the change in P^+ was too small to apply the fit. The dissociation constants obtained from the fits are 665 μM (pH 7.0), 57 μM (pH 7.4), 7.6 μM (pH 8.0), 1.3 μM (pH 8.6), and 2.1 μM (pH 9.4). Conditions: 1.5 μM reaction centers in 0.03% Triton X-100, 100 μM terbutryne, and 15 mM *N*-(2-hydroxyethyl)piperazine-*N*′-2-ethanesulfonic acid, tris(hydroxymethyl)aminomethane, or 2-(*N*-cyclohexylamino)-ethanesulfonic acid, depending on pH.

Mn^{2+} at high pH, the relative amount of P^+ is decreased as measured by the absorption change at 865 nm while the features associated with Q_A^-, notably the electrochromic shift around 760 nm, remain largely unchanged. Thus, light excitation results in formation of $P^+Q_A^-$, followed by a loss of P^+ due to oxidation of bound Mn^{2+}, with the extent measured by the decrease of the absorption change at 865 nm. The fraction of P^+ present for different manganese concentrations was used in eq 1 to determine the dissociation constant K_D. These measurements were made at pH values ranging from 6.0 to 9.5 (Figure 2B).

Above pH 8.6, the M2 mutant had a K_D value of approximately 1 μM, and the M1 and M4 mutants had larger K_D values of approximately 10 μM, consistent with the values at pH 9 reported previously (*15*). The K_D values of the M3 and M2-RY(M164) mutants were similar to the control mutant. As the pH decreased, the K_D value increased, for example, reaching a value of over 100 μM below pH 7.5 for the M2 mutant (Figure 2B). The fraction of P^+ remaining at the highest Mn^{2+} concentrations in each titration also increased as the pH decreased. The dissociation constant increased by almost 2 orders of magnitude in the M2 as well as the M1 and M4 mutants as the pH was decreased from 8 to 7 (Figure 3).

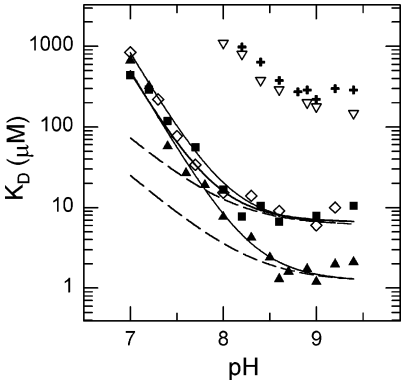

FIGURE 3: pH dependence of the dissociation constant (K_D) for manganese binding in the M1 (diamonds), M2 (triangles up), M3 (triangles down), M4 (squares), and control (cross hairs) mutants. The data points were determined for all mutants using the method shown in Figure 2. The solid lines represent the best fits using eq 3, which assumes two protonatable residues with indistinguishable pK_a values. The dissociation constants at high pH (K_D^0), where the residues would be deprotonated, are 1.2, 6.0, and 6.5 μM for the M2, M1, and M4 mutants, with pK_{ac} values of 8.30, 8.05, and 7.90, respectively. The dashed lines represent the pH dependence of K_D generated by a form of eq 3 assuming only one protonatable amino acid residue.

The pH dependence of K_D was well described using eq 3, indicating a change in the protonation state of two residues (Figure 3). The fit yielded values for K_D^0 and pK_{ac} of 1.2 μM and 8.30 for the M2 mutant, 6.0 μM and 8.05 for the M1 mutant, and 6.5 μM and 7.90 for the M4 mutant. Assuming the involvement of only one protonatable residue yielded pH dependences that agreed only at high pH values with the measured data. A small increase in the apparent K_D value was observed in the M1, M2, and M4 mutants above pH 9, presumably due to the formation of insoluble manganese hydroxide and manganese carbonate compounds, which would act as a sink for the added manganese and lower its activity. The effect became noticeable above pH 9.4, setting this pH value as the upper limit for the measurements. The data for the M3 and control mutant could not be reliably fitted as the dissociation constants remained high (>200 μM) even at alkaline pH values, suggesting only weak, nonspecific manganese binding as reported earlier for other mutants without a specific manganese-binding site (*14*).

Proton Release upon Manganese Binding in the Dark. A significant proton release was measured due to Mn^{2+} binding to the M2 mutant in the dark at pH 7.9 (Figure 4A). The amount of proton release increased significantly with increasing Mn^{2+} concentration up to a concentration of 60 μM Mn^{2+}. Under the same conditions the proton release by the control mutant showed only a moderate increase with increasing manganese concentration, presumably due to a weak and nonspecific association of manganese with the protein (*14*). Subtraction of the proton release by the control mutant from the proton release by the M2 mutant yields the proton release exclusively associated with the Mn^{2+} binding; this proton release increased from 0 to a maximum value of 1.4 H^+/RC at a concentration of 60 μM manganese.

The pH dependence of the proton release was measured for the M1, M2, M4, and control mutants (Figure 4B). The proton release from the control mutant slowly increased with increasing Mn^{2+} concentrations. In contrast, the release from the M1, M2, and M4 mutants reached a maximal value at a Mn^{2+} concentration that depended upon the pH. The concentration of the Mn^{2+} required to reach the maximal proton release was 600 μM at the lowest pH value of 6.0, decreasing to 60 μM at pH 7.9. Concentrations of 60−40 μM were needed between pH 7.9 and pH 8.4. The maximal proton release associated with the binding to each of the sites was calculated by subtracting the release in the control mutant at the corresponding Mn^{2+} concentration, and the pH dependence of the proton release associated was fit using eq 4 (Figure 4C). Assuming an *N* value of 2, the fit yielded a pK_a shift from 8.50 to 7.01 in the M2 site and a shift from 8.43 to 7.36 in the M4 site. Allowing contributions of more than two residues in the model by setting *N* as a free parameter in eq 4 resulted in a slight improvement of the fit, yielding a value of 2.77 for *N* with a pK_a shift from 8.40 to 7.20 for the M2 mutant and a value of 2.20 for *N* with a shift of 8.28 to 7.49 for the M4 mutant (fit not shown). The proton release in the M1 mutant was similar to that measured in the M4 mutant.

Light-Induced Proton Uptake/Release. The pH dependence of proton uptake/release after illumination in the M2 and control mutants was measured with and without different secondary electron donors (Figure 5). Upon illumination, both the M2 and control mutants are in the state $P^+Q_A^-$ in the absence of any secondary electron donor. Under these conditions, for the M2 mutant, the light-induced proton uptake was found to be small between pH 6.2 and pH 8.0 and then to increase to 0.3 H^+/RC as the pH was increased to 9.5 (Figure 5A). In the control mutant, the proton uptake increased gradually with increasing pH in a manner similar to that reported earlier for wild-type reaction centers, R-26 reaction centers, and a different high-potential mutant (*19*, *25*, *26*). The observed proton uptake in the $P^+Q_A^-$ state arises from a combination of proton uptake on the cytoplasmic side due to the formation of Q_A^- and proton release at the periplasmic side due to the formation of P^+. Since no modifications were made at the cytoplasmic side of the protein, the proton uptake associated with Q_A^- formation should be the same in the M2 and control mutants. Subtracting the proton uptake measured for the M2 mutant from that of the control mutant yields a proton release associated with the presence of the metal-binding site in the M2 mutant. This proton release had a maximum value of −0.15 H^+/RC at pH 8 and approached zero at both ends of the investigated pH range (Figure 5B).

In the presence of ferrocene, a fast secondary electron donor to P^+, the $P^+Q_A^-$ state generated by illumination is rapidly converted to the PQ_A^- state by electron transfer from ferrocene to P^+. The proton uptake in the presence of ferrocene was very similar for the M2 and control mutants, increasing from 0.25 to 0.40 H^+/RC as the pH increased (Figure 5C). The agreement of the proton uptake for this state in both mutants reflects the lack of interaction between the Mn^{2+}-binding site and Q_A^-. Ferrocene has been shown earlier not to contribute to the observed proton uptake/release upon oxidation (*25*). Subtracting the proton uptake generated in the presence of ferrocene (Figure 5C) from the proton uptake measured without ferrocene (Figure 5A) yields a net proton release that is due to P^+ (Figure 5D). The proton release by P^+ is seen to be larger in the M2 mutant between pH 7 and pH 9 than in the control mutant by approximately 0.1−0.15 H^+/RC.

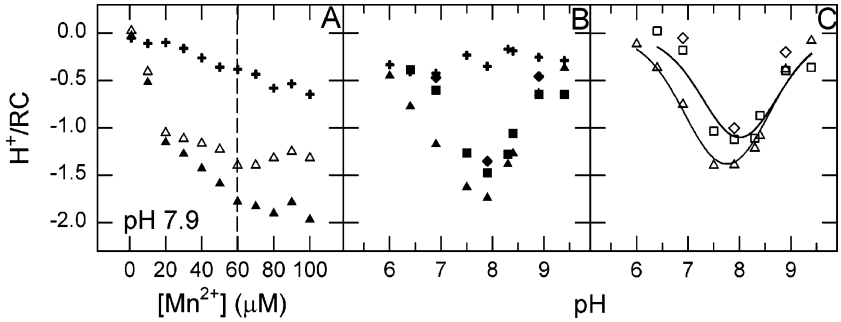

FIGURE 4: Proton release associated with the binding of Mn^{2+} to reaction centers in the dark. (A) Dependence of the proton release upon the added manganese concentration in the M2 (filled triangles) and the control mutant (cross hairs) and the difference between them (open triangles) at pH 7.9. The proton release at the M2 binding site saturates at 60 μM Mn^{2+} concentration (dashed line). (B) pH dependence of the maximal proton release in the M1 (filled diamonds), M2 (filled triangles), and M4 (filled squares) mutants as well as the release from the control mutant (cross hairs). (C) pH dependence of the calculated proton release from the M1 (open diamonds), M2 (open triangles), and M4 (open squares) binding sites. The solid curves are fits using eq 4, which assumes shifts in pK_{ac}, a single pK_a value for N coordinating residues, due to electrostatic interaction with the divalent manganese cation. For $N = 2$, pK_{ac} and δpK_{ac} values of 8.50 and -1.49 were obtained for the M2 mutant and values of 8.43 and -1.07 were obtained for the M4 mutant. Conditions: as in Figure 2 except +30 mM NaCl and ±buffers (see Materials and Methods). For panel C, the Mn^{2+} concentration ranged from 600 to 40 μM (see text).

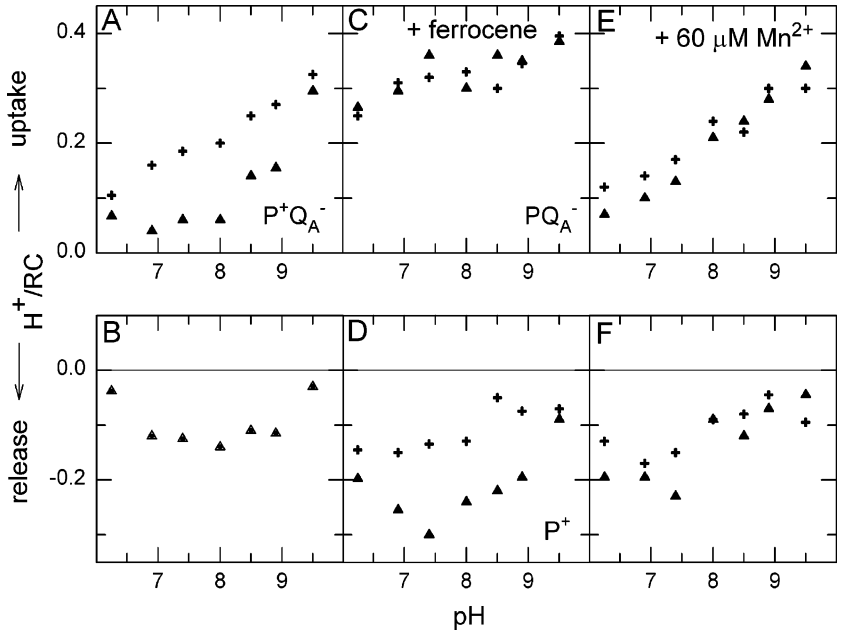

FIGURE 5: pH dependence of measured (upper panels) and calculated (lower panels) proton uptake/release in the control (cross hairs) and M2 (triangles) mutants in different light-induced states. (A) Proton uptake measured in the $P^+Q_A^-$ state generated in the absence of a secondary donor. (B) Calculated difference between the proton uptake in the M2 and control mutants in the $P^+Q_A^-$ state. This proton release is characteristic of the metal-binding site without manganese. (C) Proton uptake in the PQ_A^- state generated in the presence of 200 μM ferrocene. (D) Calculated difference between the proton uptake in the absence (panel A) and presence (panel C) of ferrocene for both mutants. The difference is the proton release associated with the formation of P^+. (E) Proton uptake in the presence of 60 μM Mn^{2+}. (F) Calculated difference between the proton uptake in the presence of manganese (panel E) and in the presence of ferrocene (panel C). Conditions: as in Figure 4 except no Mn^{2+} in panels A and C and +200 μM ferrocene in panel C.

In the presence of 60 μM $MnCl_2$, light induces a net proton uptake in the M2 and control mutants (Figure 5E). The light-induced proton uptake in both mutants is very similar in the entire investigated pH region, although different redox states are involved in these two mutants. In the control mutant, the $MnCl_2$ concentration is far below the limit where the Mn^{2+} could serve as the secondary electron donor to P^+ at any pH (Figure 3), and the measured proton uptake is the same within the experimental error as was measured without Mn^{2+} (Figure 5A). In the M2 mutant, the Mn^{2+} can serve as a secondary electron donor, and the observed proton uptake (Figure 5E) is different from that measured for the $P^+Q_A^-$ state (Figure 5A) and the PQ_A^- state (Figure 5C). The proton release due to the oxidized state alone (Figure 5F) was calculated by subtracting the values of the proton uptake due to Q_A^- as measured in the presence of ferrocene (Figure 5C) from the data in the presence of Mn^{2+} (Figure 5E). The proton release from the M2 mutant is seen to be comparable to that of the control mutant throughout the entire pH region.

DISCUSSION

In bacterial reaction centers with elevated dimer midpoint potentials, P^+ can be reduced by Mn^{2+} in a second-order reaction (*14*). In those reaction centers the Mn^{2+} can only reduce P^+ efficiently at high (millimolar) concentrations due to the lack of a high-affinity binding site. The development of a set of metal-binding sites in high-potential mutants

enables Mn^{2+} oxidation to occur at concentrations of 1−10 μM at pH 9 (*15*). In this work, these highly oxidizing reaction centers with designed manganese-binding sites were shown to have a pronounced pH dependence in their ability to bind and oxidize Mn^{2+}. The relationship between the binding and oxidation of Mn^{2+} and the accompanying proton transfer reactions can yield insight into the characteristics of the binding site.

The binding of manganese to the reaction center was found to be strongly pH dependent, with K_D values for the M2 mutant increasing from 1 μM to nearly 1 mM as the pH decreased from 9 to 7 (Figure 3). The pH dependence of K_D could be described by the participation of two titrating residues with pK_a values that are very close to each other, with the fit yielding a pK_a value of 8.3 (Figure 3). A similar pH dependence was observed for the M1 and M4 mutants (Figure 3). The effect of the protonation state of amino acid residues on the binding was corroborated by proton release measurements showing that at least two residues are required to release protons upon Mn^{2+} binding at pH 8 (Figure 4). The proton release upon binding can be explained as being the result of a downshift in the pK_a of this cluster of residues from a value of 8.5 to 7.0 as the manganese binds to the reaction centers (Figure 4C). The similarity of pK_a values derived from the pH dependence of the dissociation constant and the proton release is consistent with the model that the binding is dependent upon the protonation state of two residues serving as manganese ligands. The proton release could also include contributions from other nearby residues electrostatically interacting with the divalent cation. Similar conclusions were made for a metal-binding site near Q_B that has a strong affinity for the binding of Ni^{2+} and Cd^{2+} but not Mn^{2+} or other divalent metals (*20*, *26*). As has been previously discussed (*27*), it is difficult to determine the actual number of residues involved in electrostatic proton uptake or release because either a small number of residues with large pK_a shifts or a large number of residues with small shifts will satisfy any model. Although the identity of the proton-releasing residues is not known, the most likely candidates are those involved in the coordination of the manganese (Figure 1). Few other protonatable residues are found near the manganese-binding site.

X-ray crystallographic analysis revealed that, in the M2 mutant, the metal is coordinated by Glu M168, Glu M173, His M193, Asp M288, and a bound water molecule (Figure 1) (*15*). Although Glu M173 and His M193 are present in the wild type, manganese does not bind tightly. The lack of tight binding by manganese to the M2-RY(M164) mutant, which is identical to the M2 mutant except for the Arg to Tyr mutation at M164, shows the effect of a salt bridge interaction seen in the wild-type structure between Arg M164 and Glu M173, making Glu M173 unavailable as a ligand. In the wild type, the periplasmic surface has a broadly distributed net negative charge (Figure 6). This net negative charge facilitates the binding of cytochrome c_2 (*28*). In contrast, the M2 mutant shows a distinct localized negatively charged surface feature that is centered on the binding site created by the introduction of the Glu M168 and Asp M288 residues. This negatively charged pocket would be most pronounced at high pH. At low pH values, the residues would become protonated, greatly decreasing their contribution to the negatively charged surface feature. The decreased charge, coupled with the requirement that the protons associated with the manganese ligands must be released, could lead to the significant increase in the value of K_D at low pH values.

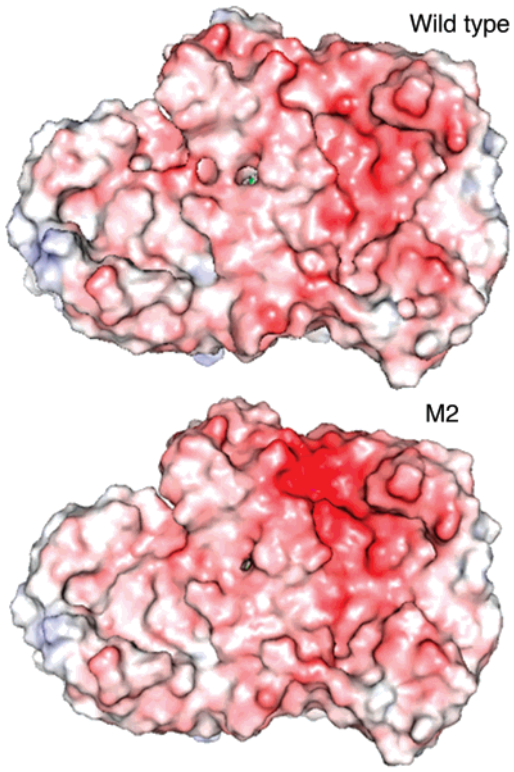

FIGURE 6: Electrostatic surface representation of the periplasmic side of the reaction center. Negatively charged regions are indicated with red, positively charged ones with blue, and neutral areas with white. In the wild type (upper), the surface has a predominately negatively charged aspect. In the M2 mutant (lower), the region where the binding site is located shows a pronounced increase in negative charge, while other areas of the electrostatic surface are largely unchanged. Coordinates for the wild type are from PDB file 1M3X, and coordinates for the M2 mutant are from PDB file 1Z9J. Surface representation made using PYMOL (*16*). View is the same as in Figure 1.

A small amount of proton release associated with the oxidized state is observed in both the M2 and control mutants at all pH values (Figure 5). It has been shown in earlier studies that proton release at the periplasmic side of the reaction center due to the formation of P^+ is very limited above pH 8 (*19*, *25*, *26*). The proton release due to P^+ in the M2 mutant is increased slightly compared to the control, most likely because of proton release from the introduced carboxylate groups in response to P^+, although other nearby residues may additionally have altered electrostatic interactions in the M2 mutant. This increase is presumably due to a partial release of protons either directly from the introduced carboxylates or from residues near the carboxylates that become protonated in the mutant due to shifts in their pK_a values arising from electrostatic interactions with the carboxylates. The amount of proton release due to Mn^{3+} at high pH in the M2 mutant is similar to the proton release due to P^+ in the control mutant, indicating that the change in position of the charge from P to the Mn-binding site does not alter the electrostatic response of the protein. The lack of a large amount of proton uptake in the M2 mutant in the presence of manganese at high pH indicates that the manganese remains bound after illumination. If the manga-

nese did not remain bound, an uptake of the two protons that were observed to be released upon binding of the manganese in the dark would be expected (Figure 4). However, the results do not distinguish between the Mn^{3+} remaining bound and a rapid exchange with Mn^{2+} in solution.

In addition to altering the binding affinity, lowering the pH apparently results in an incomplete manganese oxidation reaction, as evidenced by the increase in the fraction of P^+ present at high concentrations of manganese (Figure 2B). The incomplete reaction is likely due to a decrease in the free energy difference at lower pH values. At high Mn^{2+} concentrations, all of the reaction centers should have bound manganese; however, a fraction of reaction centers will be in the state Mn^{2+} $P^+Q_A^-$ after illumination if the free energy difference for the transfer of an electron from the manganese to P^+ is close to zero or positive. For example, at pH 7.0 the fraction of P^+ remaining at high Mn^{2+} concentration is approximately half, suggesting that the free energy difference is substantially decreased compared to its value at pH 9.4. Since the P/P^+ midpoint potential in the wild type and the carotenoidless R-26 mutant is only slightly pH dependent, with an average slope of −6 mV/pH between pH 7 and pH 10 (*25*, *29*), the pronounced pH dependence probably arises from a change in the oxidation/reduction midpoint potential of the manganese. For manganese in solution, the midpoint potential exhibits a strong pH dependence with a slope of close to −60 mV/pH (*14*).

In summary, the binding of Mn^{2+} to the M2 site on the reaction center was shown to be strongly dependent upon the protonation state of the residues at the binding site, as demonstrated by the pH dependence of the dissociation constant and the proton release upon binding. At low pH, two residues are modeled as being protonated, resulting in weak binding of Mn^{2+}. At pH 8, the residues are poised such that Mn^{2+} binding is accompanied by the release of two protons. At high pH, the residues are deprotonated, and Mn^{2+} readily binds. These results show that both the configuration and the protonation state of the residues designed to serve as ligands need to be considered in the construction of new metal-binding sites in proteins.

ACKNOWLEDGMENT

We thank Lisa Lauman for assistance with the growth of the bacterial cells and Rebecca Dowler for help in mutagenesis.

REFERENCES

1. Sundaramoorthy, M., Kishi, K., Gold, M. H., and Poulos, T. L. (1994) The crystal structure of manganese peroxidase from *Phanerochaete chrysosporium* at 2.06-Å resolution, *J. Biol. Chem. 269*, 32759−32767.
2. Bewley, M. C., Jeffrey, P. D., Patchett, M. L., Kanyo, Z. F., and Baker, E. N. (1999) Crystal structures of *Bacillus caldovelox* arginase in complex with substrate and inhibitors reveal new insights into activation, inhibition and catalysis in the arginase superfamily, *Structure 7*, 435−448.
3. Goedken, E. N., and Marqusee, S. (2001) Co-crystal of *Escherichia coli* RNase HI with Mn^{2+} ions reveals two divalent metals bound in the active site, *J. Biol. Chem. 276*, 7266−7271.
4. Allen, J. P., Feher, G., Yeates, T. O., Komiya, H., and Rees, D. C. (1987) Structure of the reaction center from *Rhodobacter sphaeroides* R-26: The protein subunits, *Proc. Natl. Acad. Sci. U.S.A. 84*, 6162−6166.
5. Zouni, A., Witt, H. T., Kern, J., Fromme, P., Krauss, N., Saenger, W., and Orth, P. (2001) Crystal structure of photosystem II from *Synechococcus elongatus* at 3.8 Å resolution, *Nature 409*, 739−743.
6. Blankenship, R. E., Madigan, M. T., and Bauer, C. E., Eds. (1995) *Anoxygenic Photosynthetic Bacteria*, Kluwer Academic Publishers, Dordrecht, The Netherlands.
7. Ort, D. R., and Yocum, C. F., Eds. (1996) *Oxygenic Photosynthesis: The Light Reactions*, Kluwer Academic Publishers, Dordrecht, The Netherlands.
8. Lin, X., Murchison, H. A., Nagarajan, V., Parson, W. W., Allen, J. P., and Williams, J. C. (1994) Specific alteration of the oxidation potential of the electron donor in reaction centers from *Rhodobacter sphaeroides*, *Proc. Natl. Acad. Sci. U.S.A. 91*, 10265−10269.
9. Kálmán, L., LoBrutto, R., Allen, J. P., and Williams, J. C. (1999) Modified reaction centres oxidize tyrosine in reactions that mirror photosystem II, *Nature 402*, 696−699.
10. Narváez, A. J., Kálmán, L., LoBrutto, R., Allen, J. P., and Williams, J. C. (2002) Influence of the protein environment on the properties of a tyrosyl radical in reaction centers from *Rhodobacter sphaeroides*, *Biochemistry 41*, 15253−15258.
11. Narváez, A. J., LoBrutto, R., Allen, J., P., and Williams, J. C. (2004) Trapped tyrosyl radical populations in modified reaction centers from *Rhodobacter sphaeroides*, *Biochemistry 43*, 14379−14384.
12. Kálmán, L., LoBrutto, R., Narváez, A. J., Williams, J. C., and Allen, J. P. (2003) Correlation of proton release and electrochromic shifts of the optical spectrum due to oxidation of tyrosine in reaction centers from *Rhodobacter sphaeroides*, *Biochemistry 42*, 13280−13286.
13. Kálmán, L., Narváez, A. J., LoBrutto, R., Williams, J. C., and Allen, J. P. (2004) Dependence of tyrosine oxidation in highly oxidizing bacterial reaction centers on pH and free-energy difference, *Biochemistry 43*, 12905−12912.
14. Kálmán, L., LoBrutto, R., Allen, J. P., and Williams, J. C. (2003) Manganese oxidation by modified reaction centers from *Rhodobacter sphaeroides*, *Biochemistry 42*, 11016−11022.
15. Thielges, M., Uyeda, G., Cámara-Artigas, A., Kálmán, L., Williams, J. C., and Allen, J. P. (2005) Design of a redox-linked active metal site: manganese bound to bacterial reaction centers at a site resembling that of photosystem II, *Biochemistry 44*, 7389−7394.
16. DeLano, W. L. (2002) *The PyMOL Molecular Graphics System*, DeLano Scientific, San Carlos, CA.
17. Paddock, M. L., Rongey, S. H., Feher, G., and Okamura, M. Y. (1989) Pathway of proton-transfer in bacterial reaction centers: Replacement of glutamic acid 212 in the L-subunit by glutamine inhibits quinone (secondary acceptor) turnover, *Proc. Natl. Acad. Sci. U.S.A. 86*, 6602−6606.
18. Williams, J. C., Alden, R. G., Murchison, H. A., Peloquin, J. M., Woodbury, N. W., and Allen, J. P. (1992) Effects of mutations near the bacteriochlorophylls in reaction centers from *Rhodobacter sphaeroides*, *Biochemistry 31*, 11029−11037.
19. Kálmán, L., Williams, J. C., and Allen, J. P. (2003) Proton release upon oxidation of tyrosine in reaction centers from *Rhodobacter sphaeroides*, *FEBS Lett. 545*, 193−198.
20. Gerencsér, L., and Maróti, P. (2001) Retardation of proton transfer caused by binding of the transition metal ion to the bacterial reaction center is due to pK_a shifts of key protonatable residues, *Biochemistry 40*, 1850−1860.
21. Straley, S. C., Parson, W. W., Mauzerall, D. C., and Clayton, R. K. (1973) Pigment content and molar extinction coefficients of photochemical reaction centers from *Rhodopseudomonas spheroides*, *Biochim. Biophys. Acta 305*, 597−609.
22. Kleinfeld, D., Okamura, M. Y., and Feher, G. (1985) Electron transfer in reaction centers of *Rhodopseudomonas sphaeroides*. II. Free energy and kinetic relations between the acceptor states $Q_A^-Q_B^-$ and $Q_AQ_B^{2-}$, *Biochim. Biophys. Acta 809*, 291−310.
23. Maróti, P., Kirmaier, C., Wraight, C. A., Holten, D., and Perlstein, R. M. (1985) Photochemistry and electron transfer in borohydride-treated reaction centers, *Biochim. Biophys. Acta 810*, 132−139.
24. Paddock, M. L., Sagle, L., Tehrani, A., Beatty, J. T., Feher, G., and Okamura, M. Y. (2003) Mechanism of proton-transfer inhibition by Cd^{2+} binding to bacterial reaction centers: Determination of the pK_A of functionally important histidine residues, *Biochemistry 42*, 9626−9632.
25. Maróti, P., and Wraight, C. A. (1988) Flash-induced H^+ binding by bacterial photosynthetic reaction centers: Influences of the

redox states of the acceptor quinones and primary donor, *Biochim. Biophys. Acta 934*, 329−347.
26. Paddock, M. L., Graige, M. S., Feher, G., and Okamura, M. Y. (1999) Identification of the proton pathway in bacterial reaction centers: inhibition of proton transfer by binding of Zn^{2+} or Cd^{2+}, *Proc. Natl. Acad. Sci. U.S.A. 96*, 6183−6188.
27. McPherson, P. H., Okamura, M. Y., and Feher, G. (1988) Light-induced proton uptake by photosynthetic reaction centers from *Rhodobacter sphaeroides* R-26. I. Protonation of the one-electron states $D^+Q_A^-$, DQ_A^-, $D^+Q_AQ_B^-$, and $DQ_AQ_B^-$, *Biochim. Biophys. Acta 934*, 348−368.
28. Axelrod, H. L., and Okamura, M. Y. (2005) The structure and function of the cytochrome c_2: reaction center electron transfer complex from *Rhodobacter sphaeroides*, *Photosynth. Res. 85*, 101−114.
29. Williams, J. C., Haffa, A. L. M., McCulley, J. L., Woodbury, N. W., and Allen, J. P. (2001) Electrostatic interactions between charged amino acid residues and the bacteriochlorophyll dimer in reaction centers from *Rhodobacter sphaeroides*, *Biochemistry 40*, 15403−15407.

BI051149W